A feasibility study on microwave imaging of bone for osteoporosis monitoring

Amin, Bilal; Shahzad, Atif; Crocco, Lorenzo; Wang, Mengchu; O'Halloran, Martin; González-Suárez, Ana; Elahi, Muhammad Adnan

DOI:
10.1007/s11517-021-02344-8

A feasibility study on microwave imaging of bone for osteoporosis monitoring

Bilal Amin[1,2], Atif Shahzad[3,4], Lorenzo Crocco[5], Mengchu Wang[5], Martin O'Halloran[1,2,3], Ana González-Suárez[1,2], and Muhammad Adnan Elahi[1,2]

[1]Electrical and Electronic Engineering, National University of Ireland Galway, Ireland

[2]Translational Medical Device Lab, National University of Ireland Galway, Ireland

[3]School of Medicine, National University of Ireland Galway, Ireland

[4]Centre for Systems Modelling and Quantitative Biomedicine, Institute of Metabolism and Systems Research, University of Birmingham, United Kingdom

[5]IREA-CNR, Institute for Electromagnetic Sensing of the Environment, National Research Council of Italy, Naples, Italy

Address: Translational Medical Device Lab, Lambe Institute for Translational Research & HRB Clinical Research Facility, University Hospital Galway

Corresponding Author Email: b.amin2@nuigalway.ie

Corresponding Author Telephone: +35389-9802534

Corresponding Author Fax: N/A

Total number of words of the manuscript: 6998

Number of words of the abstract: 205

Number of figures: 10

Number of tables: 2

Abstract
The dielectric properties of bones are found to be influenced by the demineralisation of bones. Therefore, microwave imaging (MWI) can be used to monitor *in vivo* dielectric properties of human bones and hence aid in the monitoring of osteoporosis. This paper presents the feasibility analysis of the MWI device for monitoring osteoporosis. Firstly, the dielectric properties of tissues present in the human heel are analysed. Secondly, a transmission line (TL) formalism approach is adopted to examine the feasible frequency band and the matching medium for MWI of trabecular bone. Finally, simplified numerical modelling of the human heel was set to monitor the penetration of E-field, the received signal strength, and the power loss in a numerical model of the human heel. Based on the TL formalism approach, 0.6 – 1.9 GHz frequency band is found to feasible for bone imaging purpose. The relative permittivity of the matching medium can be chosen between 15 – 40. The average percentage difference between the received signal for feasible and inconvenient frequency band was found to be 82%. The findings based on the dielectric contrast of tissues in the heel, the feasible frequency band, and the finite difference time domain simulations support the development of an MWI prototype for monitoring osteoporosis.

Keywords: Dielectric Properties, Feasible Frequency Band, Microwave Imaging, Numerical Modelling, Osteoporosis.

1. INTRODUCTION

Osteoporosis is a major bone disease, caused due to progressive demineralisation of bones that deteriorates the trabecular bone microarchitecture, and hence leads to bone fragility and fractures [23],[11]. Annually, 8.9 million fractures are reported worldwide due to osteoporosis [10]. Osteoporosis is considered the most commonly encountered bone disease in the US, as it almost affects 50% of American women and 25% of men over the age of 50 years [26]. Due to the ageing population in the EU, osteoporotic fractures are expected to be doubled by 2050 and hence will overall impact the economic burden to $25.3 billion [8]. Bone mineral density (BMD) is considered a key clinical indicator to monitor osteoporosis and is widely accepted in clinics for its diagnosis [29]. Currently, a dual-energy X-ray absorptiometry (DXA) scan is employed to measure the BMD of the trabecular bone [29],[20]. However, DXA is not cost-effective, as the scan is time-consuming and the device is not portable. Moreover, DXA uses ionising radiations, and therefore frequent DXA scans are associated with long term health risks [22]. Therefore, alternative imaging technologies such as microwave imaging (MWI) have targeted trabecular bone evaluation to replace DXA in the overall diagnosis of osteoporosis [16].

MWI is an emerging diagnostic technology being investigated for a range of medical applications such as breast cancer detection and diagnosing brain stroke [33],[25],[32]. The key advantages of MWI for diagnosing and monitoring various diseases compared to existing imaging modalities are non-ionising radiations, portability, and low cost [3]. Recent studies have investigated the feasibility of using MWI for osteoporosis monitoring [1],[22],[12] based on the notable difference between dielectric properties of healthy and diseased human trabecular bones [2],[5],[6]. The associated clinical advantages and the difference of dielectric properties between healthy and diseased human trabecular bones make MWI a potential imaging modality for monitoring bone health in comparison to the DXA [5],[21]. MWI can be classified into two main categories: radar-based and tomographic MWI [7]. In radar-based MWI techniques, images are constructed based on the scattered waves that arise due to the dielectric contrast between normal and malignant tissues [30]. The radar-based techniques are mainly used to localize any strong scatterer/pathology in the biological tissues without reconstructing the full image of biological tissues [27]. Contrary to this, the tomographic MWI techniques aim at retrieving

the spatial distribution of dielectric properties (relative permittivity (ε_r) and conductivity ($\sigma(S/m)$)) of biological tissues by processing measured scattered electromagnetic (EM) field data [33].

A comprehensive review of bone dielectric properties in the microwave frequency range was reported by Amin *et al.* [1]. This review reported that only two studies to date have measured the dielectric properties of human trabecular bones, which suggests that limited work has been done on this topic. Meaney *et al.* [22] reported *in vivo* dielectric properties of human calcaneus bone by using microwave tomography (MWT) for a frequency range of 900 - 1700 MHz. In this study, the authors have used their breast imaging prototype for imaging the human heel of two patients suffering from a lower leg injury and achieved promising results [22]. However, a dedicated MWI system for bone imaging application would further improve their results for monitoring osteoporosis. The second study was performed by Irastorza *et al.* [18], in which the authors have measured *in vitro* dielectric properties of normal human trabecular bones extracted from patients undergoing total hip replacement surgeries by using open-ended coaxial line (OECL) probes in the frequency range of 100 - 1300 MHz. In another study, Amin *et al.* [5] reported *in vitro* dielectric properties of diseased human trabecular bones extracted also from patients undergoing total hip replacement surgeries by using OECL probes in a frequency range of 0.5 - 8.5 GHz. Amin *et al*. [5] also performed a comparison between diseased human trabecular bones with different bone volume fraction finding a significant dielectric variation between osteoporotic and osteoarthritis human trabecular bone samples.

Despite the promising initial evidence that dielectric properties can be potentially used for osteoporosis diagnosis, no dedicated MWI system exists to measure *in vivo* dielectric properties of human bone in the microwave frequency range. Some of the important initial steps towards the development of an MWI system for bone imaging require the knowledge of the optimal frequency band, the appropriate matching medium for maximum EM field penetration, and the development of numerical bone models to be adopted in the validation. Therefore, this study aims to investigate these issues to assess the feasibility of MWI for imaging bones and monitoring osteoporosis and osteoarthritis and will accelerate the development of prototype systems and algorithms to image the dielectric properties of bone for diagnostic purposes.

The application of MWI for the reconstruction of dielectric properties of target tissue primarily depends upon the dielectric contrast between the target and its surrounding tissues. The target tissue for bone imaging application to monitor osteoporosis is trabecular bone, as osteoporosis continuously deteriorates the trabecular bone microarchitecture, which makes the bone fragile causing fractures [10]. Moreover, the trabecular bones (inner part of the bone) have a spongier pattern than the cortical bones (hard exterior part of the bone), thus trabecular bones are more prone to osteoporotic fractures [26]. Therefore, firstly, this study has collated and analysed the dielectric properties of various human heel tissues from the literature. The human heel is composed of skin, fat, muscle, cortical bone, and trabecular bone. The dielectric contrast of heel tissues will determine whether the trabecular bone can be distinguished based on the dielectric properties from other tissues present in the heel. Once the dielectric contrast of heel tissues was established, a transmission line (TL) formalism approach as the one adopted in [32] for MWI applied to cerebrovascular diseases was adopted for finding feasible frequency band for bone imaging applications as well as a proper matching medium. The electric field (E-field) penetration, the received signal strength, and the power loss were analysed for this feasible frequency band and the proposed matching medium. In this analysis, simplified numerical modelling of the human heel was exploited.

The finite difference time domain (FDTD) simulations were performed using numerical models of the heel, which was modelled as a five-layered cylinder composed of: skin, fat, muscle, cortical bone,

and trabecular bone. Further, to analyse the feasible frequency band for osteoporotic and osteoarthritis bone samples, the dielectric properties of the trabecular bone layer in the five-layered cylindrical model were modified based on the dielectric properties of osteoporotic and osteoarthritis bone samples as reported by Amin *et al.* [5]. The trabecular bone microarchitecture of osteoarthritis patients is compact and dense compared to osteoporotic patients [35]. The dense trabecular microarchitecture of bone indicates a higher degree of mineralisation due to the greater amount of bone present [22],[23]. Therefore, the bone samples from osteoarthritis and osteoporotic patients allows establishing the variation in bone dielectric properties due to variation in mineralisation content and microarchitecture between two diseased bones [4]. Once an optimal frequency band was determined, the matching medium dielectric properties were selected based on the feasible frequency band. An optimum choice for matching medium helps to improve the coupling between the incident wave and the tissues. In summary, this study has investigated: the dielectric contrast of human heel tissues; suitable frequency band for bone imaging; appropriate matching medium for maximum EM field penetration in the heel; numerical model of the human heel, and validation of selected frequency band in terms of E-field penetration in the trabecular bone, received signal strength across the numerical model of the heel, and power loss across simple but realistic human heel imaging scenario. The findings of this study support the development of an MWI prototype for monitoring osteoporosis.

The remainder of the paper is organized as follows: Section 2 discusses the methodology adopted to address the objectives of this study; Section 3 discusses the results involving dielectric properties contrast of heel tissues, design guidelines for the imaging device, which involves the choice of the matching medium, the frequency range, the numerical modelling of the human heel, and the CST simulations performed on a numerical model of human heel; and finally, conclusions are drawn in Section 4.

2. METHODS

A. Dielectric properties contrast of tissues present in the heel

The application of MWI for reconstructing the dielectric properties of biological tissues primarily depends upon the dielectric contrast between the tissues of the target anatomical site. Therefore, to diagnose osteoporosis the trabecular bone should exhibit a dielectric contrast to other tissues present in the heel and their contrast between different heel tissues was investigated. The tissues considered for modelling the human heel were skin, fat, muscle, cortical bone, and trabecular bone. The dielectric measurement data of considered tissues was acquired from Gabriel *et al*. [15] for a frequency range of 0.5 – 5 GHz. Gabriel *et al*. [15]'s study is the most comprehensive study widely used for characterising the dielectric properties of tissue measured under a similar experimental setup. Moreover, to analyse the penetration depth of EM waves as a function of frequency, the skin depth of considered tissues is analysed. The skin depth data of considered tissues were acquired from Gabriel *et al*. [14] for a frequency range of 0.5 – 5 GHz. Gabriel *et al*. [14] have presented the skin depth of various biological tissues as a function of frequency. The data acquired from Gabriel *et al*. [14] was plotted in MATLAB (The MathWorks, Natick, MA, USA). The anatomical structure of the human heel and the structure of bone is shown in Figure 1 (a) and Figure 1 (b) respectively.

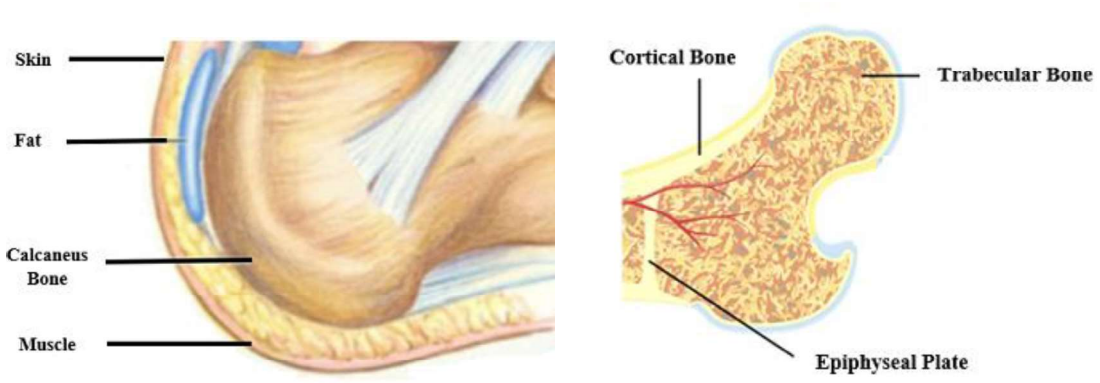

(a) **(b)**

Fig. 1(a) Anatomical structure of human heel (© 2014 WebMD, LLC. All rights reserved) **(b)** Anatomical structure of bone

B. On the choice of frequency range and the matching medium

The choice of frequency range and matching medium's relative permittivity suitable for the design of an MWI device for bone health monitoring is performed by adopting the TL formalism approach as in [32]. These two parameters represent the degrees of freedom of the MWI device [31], the choice of these parameters should be performed to impact the following two objectives:

1. Maximum incident power should penetrate the target tissue (in our case the trabecular bone)
2. The spatial resolution should be maximum to detect the small variations in the target tissue

The frequency range and the matching medium properties dictate the wavelength of the EM wave and hence the spatial resolution achieved by MWI [34]. Moreover, the choice of the relative permittivity of the matching medium determines, from each frequency, the EM wave penetration into the medium under investigation, the higher the matching between electrical discontinuities, the higher the EM penetration would be.

To address these choices, a planar layered model and a cylindrical layered model were investigated. The planar layered model allows for the use of the TL formalism approach and it is therefore convenient for a first-order analysis which is then validated numerically with the cylindrical layered model [31]. The TL formalism approach helps to identify the feasible frequency band based on the transmission coefficient (T). In TL formalism approach, the anatomical site to be imaged is modelled as one-dimensional (1-D) planar layered model, where each layer is assigned with an equivalent impedance (Z) [32]. The penetration of EM waves into trabecular bone can be assessed from the strength of the transmission coefficient. Moreover, the choice of matching medium's relative permittivity is dictated based on the feasible frequency band.

1) Planar layered model

The planar layered model approach models the heel as a 1-D layered structure. The probing wave (E_{inc}) which impacts the 1-D structure is modelled as a plane wave with normal incidence. The 1-D heel structure of the human heel is composed of five layers: skin, fat, muscle, cortical bone, and trabecular bone as shown in Figure 2. Based on the empirical studies and average statistics of the thickness of human biological tissues the thickness of skin, fat, and cortical bone was taken equal to 3.5 mm [28], 5 mm [32], and 3 mm [13] respectively. While the thickness of other layers is based on the values reported in the literature, the thickness of the muscle is assumed to be 6 mm (slightly greater than the fat). The trabecular bone was modelled as half-space to ensure maximum penetration of the EM field. Each layer

was assigned the dielectric properties of the corresponding tissue layer. The 1-D numerical modelling and FDTD simulations were performed with MATLAB (The MathWorks, Natick, MA, USA).

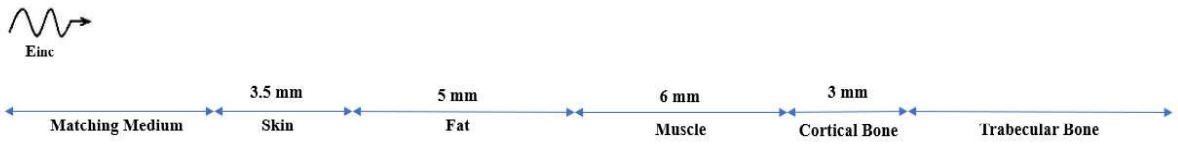

Fig. 2 The 1-D planar layered model of the human heel, which is composed of five layers: skin, fat, muscle, cortical bone, and trabecular bone. E_{inc} is the probing wave

To investigate the propagation of the EM wave using the TL formalism, each tissue layer is modelled as impedance as shown in Figure 3. The impedances $Z_{mm}, Z_s, Z_f, Z_m, Z_{CB}$, and Z_{TB} represent impedance of matching medium, skin, fat, muscle, cortical bone, and trabecular bone respectively. The trabecular bone represents the load of the TL circuit. The impedance of any specific tissue layer (Z_n) is modelled as:

$$Z_n = \sqrt{\frac{\mu_o}{\varepsilon_o \varepsilon_n}} \qquad (1)$$

where ε_n denotes the complex permittivity of the tissue layer under consideration, $\mu_o$and ε_o denote permeability and relative permittivity of free space respectively. The amount of incident power captured by the heel can be modelled by using the transmission coefficient and is given as:

$$T = 1 - \Gamma \ , \qquad (2)$$

where Γ denotes the reflection coefficient at plane HH' (interface between the matching medium and the heel). The reflection coefficient is given as:

$$\Gamma = \frac{Z_{HH'} - Z_{mm}}{Z_{HH'} + Z_{mm}} \qquad (3)$$

where Z_{mm} denotes the impedance of matching medium and $Z_{HH'}$ denotes the impedance of the plane HH'.

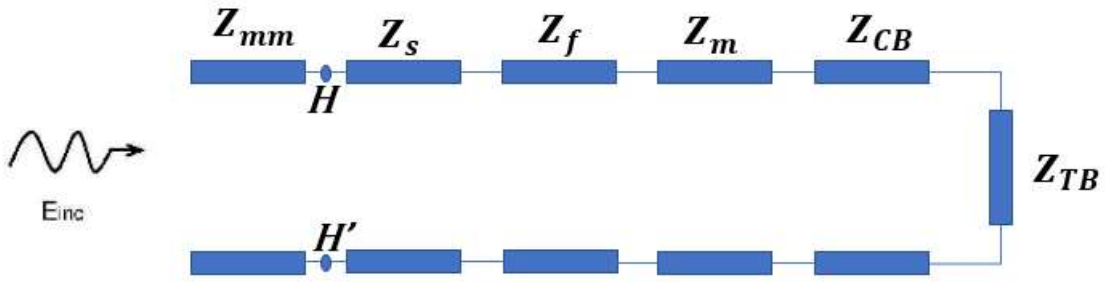

Fig. 3 The transmission line model of 1-D heel structure. The $Z_{mm}, Z_{HH'}, Z_s, Z_f, Z_m, Z_{CB}$, and Z_{TB} represent impedance of matching medium, plane HH', skin, fat, muscle, cortical bone, and trabecular bone respectively

2) Cylindrical layered model

To assess the validity of the outcomes (feasible frequency band and matching medium permittivity) of the TL analysis with a more realistic (while still simple) model, a five-layered cylindrical heel model was designed as shown in Figure 4. The choice of cylindrical layered model is used because the shape of the human heel resembles closely a cylinder. The validity was assessed in terms of E-field penetration

into trabecular bone, the amplitudes of the received signal, and the power loss in the five-layered heel structure. The objective of the numerical modelling was to assess the validity of the feasible frequency band obtained by the TL analysis. Therefore, a single frequency of 1.3 GHz was selected from the feasible frequency band (0.6 – 1.9 GHz) and FDTD simulations were then performed at the selected frequency of 1.3 GHz. Therefore, each layer of the model was assigned with a relative permittivity and conductivity of the corresponding tissue of the human heel at 1.3 GHz as acquired from Gabriel *et al.* [15]. The thickness and dielectric properties of each layer are tabulated in Table 1.

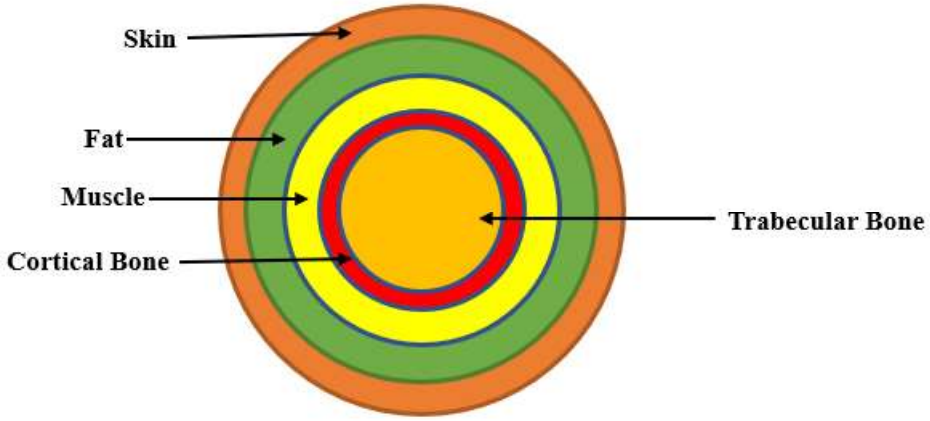

Fig. 4 A five-layered human heel model

Table 1. Dielectric properties and thickness of considered tissues of the human heel. The dielectric properties are reported at 1.3 GHz. The values are taken from Gabriel *et al.* [15]

Tissue	Relative Permittivity	Conductivity $[S/m]$	Thickness[mm]
Skin	39.917	1.0009	3.5
Fat	5.4073	0.061787	5
Muscle	54.268	1.0973	6
Cortical Bone	12.124	0.19638	3
Trabecular Bone	20.06	0.44158	15

To assess the E-field penetration for osteoporotic and osteoarthritis bones, the dielectric properties of the trabecular bone layer for the five-layered cylindrical model were modified. The values of relative permittivity and conductivity for osteoporotic and osteoarthritis bones were acquired from Amin *et al.* [5]. The values of relative permittivity and conductivity for osteoporotic and osteoarthritis bones at 1.3 GHz are tabulated in Table 2. The numerical modelling and FDTD simulations were performed in computer simulation technology software (CST MWS Suite 2018, Dassault Systemes, France).

Table 2. Dielectric Properties of osteoporotic and osteoarthritis human trabecular bone samples at 1.3 GHz

Bone Sample	Relative Permittivity	Conductivity $[S/m]$
Osteoporotic	18.2981	0.4746
Osteoarthritis	28.0299	0.6705

To validate the feasible frequency band, the five-layered cylindrical model was excited by using four waveguide ports having transverse magnetic (TM) propagation. These waveguide ports sequentially illuminated the cylindrical model with a modulated wideband Gaussian pulse. The waveguide ports were placed circularly at equidistant from each other around the cylindrical model. The simulation box had a size of 125 mm × 50 mm × 125 mm and a total of 370,881 mesh cells. The minimum and maximum mesh cell sizes are 1 mm and 1.86045 mm respectively. The perfectly matched

layer (PML) boundary conditions were used in the simulation. The minimum distance of PML to the simulating structure is 4 fractions wavelength. The FDTD simulation was performed in CST and the received signal strength between two waveguide ports placed around the five-layered cylindrical model was analyzed.

3. RESULTS AND DISCUSSION

This section firstly presents an analysis of the comparison of dielectric properties of considered tissues in the heel. Then, the TL formalism approach is presented to investigate the feasible frequency band of the MWI system for bone imaging application considering the human heel as our target anatomical site. The peripheral location of the human calcaneus bone and a similar ratio of cortical to the trabecular bone as found in the femoral head and lumbar spine makes it suitable for bone health monitoring [22],[36],[24]. The femoral head and lumbar spine are primary targets for standard osteoporosis monitoring technologies [36].

A. Dielectric properties contrast of tissues present in the heel

Figure 5 shows the dielectric properties of all considered tissues present in the heel. The dielectric data is acquired from Gabriel *et al*. [15]'s database for the 0.5 – 5 GHz frequency band. The dielectric profile of tissues suggests that a significant amount of contrast exists in terms of relative permittivity and conductivity among all tissues present in the heel. More precisely, as it can be observed from Figure 5 that the dielectric properties of trabecular bone can be well distinguished from the dielectric properties of other tissues present in the heel. The average percentage difference between the relative permittivity and conductivity of the skin and trabecular bone is found to be 70% and 56% respectively, whereas the average percentage difference between the relative permittivity and conductivity of trabecular bone and cortical bone is found to 48% and 65% respectively, across 0.5 – 5 GHz. The presence of enough dielectric contrast between heel tissues assures that MWI can be employed to distinguish and to reconstruct the dielectric properties of trabecular bone.

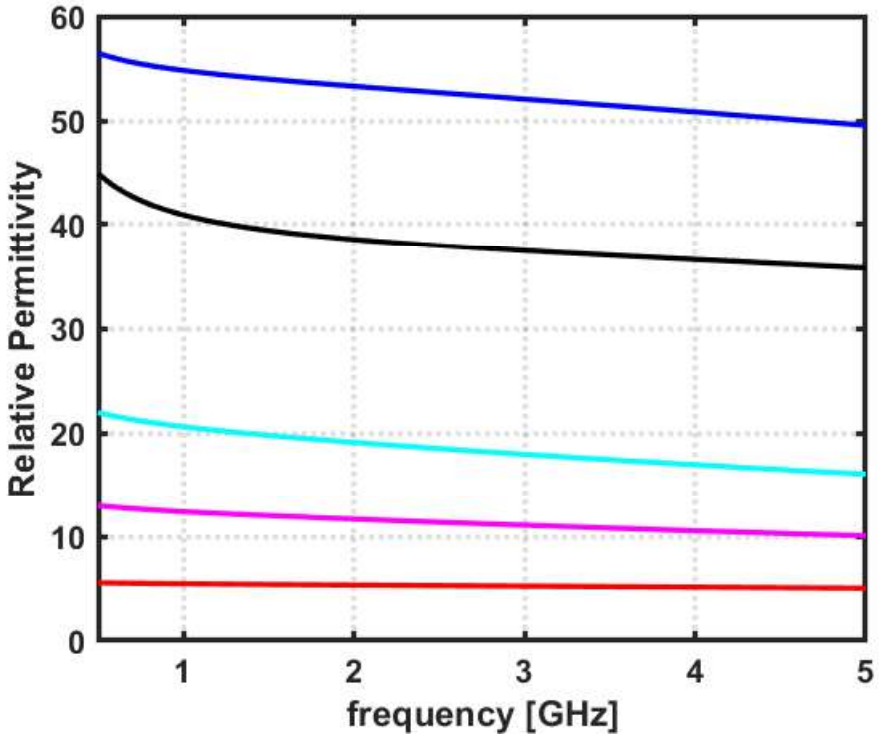

(a)

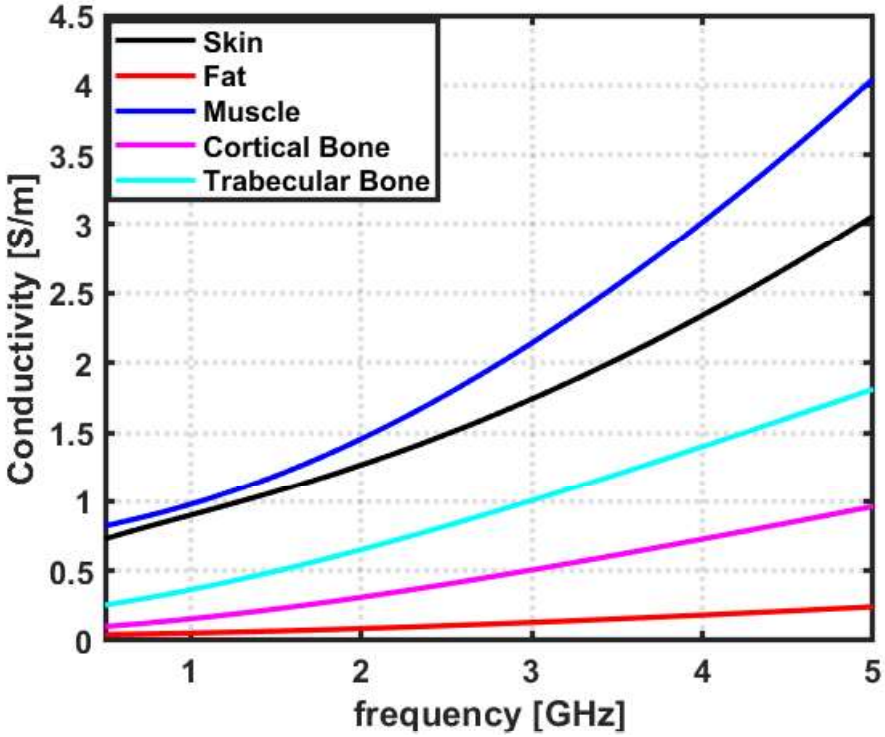

(b)

Fig. 5 Dielectric properties of considered tissues in human heel: **(a)** Relative Permittivity; **(b)** Conductivity. The values are taken from Gabriel *et al*. [15]

B. On the Choice of Frequency Range and the Matching Medium

1) Planar Layered Model

To determine the feasible frequency band and relative permittivity of the matching medium, the transmission coefficient is evaluated as a function of frequency (0.5 – 5 GHz) as shown in Figure 6. It can be observed from Figure 6, that a frequency band exists between 2 – 3.5 GHz, where the transmission coefficient is significantly less. The magnitude of the transmission coefficient in the 2 – 3.5 GHz range is comparatively lower compared to 0.6 – 1.9 GHz, hence the operating conditions of the MWI device does not seem favourable in this frequency range.

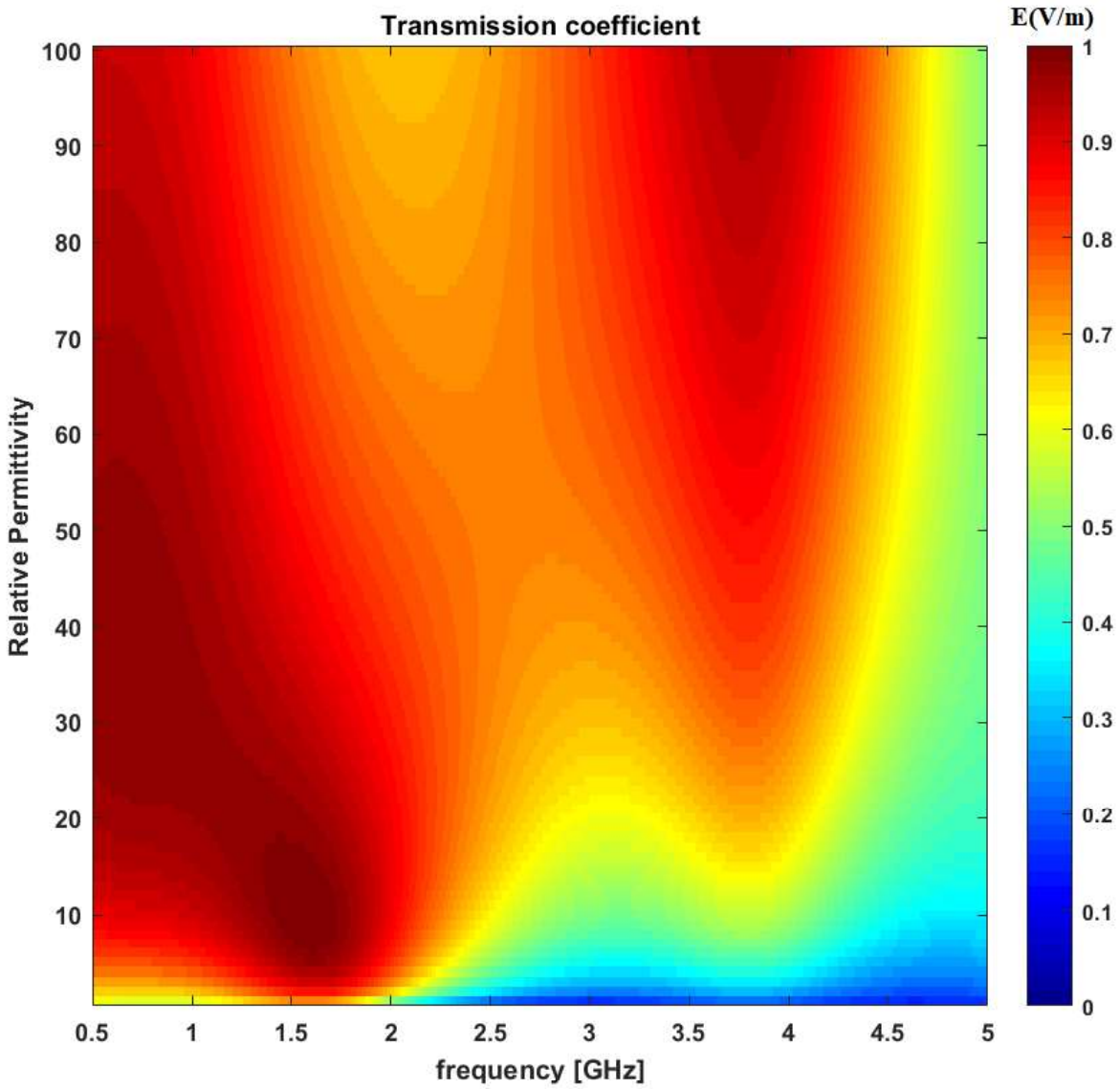

Fig. 6 The transmission coefficient as a function of frequency and relative permittivity of the matching medium

The 2 – 3.5 GHz frequency range is less convenient for the MWI device. The value of the transmission coefficient is less in the 2 – 3.5 GHz frequency range, this is because a noticeable difference exists in terms of dielectric properties of each layer considered in the five-layered heel model. In addition to this, the electrical length of low permittivity tissue layers such as fat and cortical bone causes a strong mismatch. It can be observed that the magnitude of the transmission coefficient is strong beyond 3 GHz. However, the low penetration depth of all considered tissues beyond 2.5 GHz makes 3 GHz less favourable for the MWI device. Taking all these considerations, 0.6 – 1.9 GHz would be the most appropriate frequency range for MWI of the human heel for bone health monitoring. Regarding the choice of relative permittivity for matching medium, it can be observed from Figure 6 that any value of relative permittivity can be chosen between 15 – 40 for a frequency range of 0.6 – 1.9 GHz. The value of relative permittivity greater than 40 results in a higher frequency range. As the spatial resolution depends upon the wavelength in the background medium, therefore, a matching medium having a large value of relative permittivity will be preferable [34]. The choice of matching medium primarily depends upon factors such as conductive loss, relative permittivity, antenna matching, and ease of use [17]. Therefore, an oil/water emulsion can be prepared to achieve a conductivity of 0.05 S/m and relative

permittivity of 23 [17]. Other fluids including safflower oil, glycerin, and acetone can also be used as a matching medium to achieve similar relative permittivity and conductivity [17].

The penetration of EM waves in human biological tissues reduces as a function of frequency. To investigate the feasible frequency band based on the penetration of EM waves, data is acquired from Gabriel *et al*. [14] for considered tissues present in the heel. Figure 7 depicts the penetration of EM fields for the observed frequency band (0.5 – 5 GHz). It can be observed from Figure 7 that the penetration of EM fields reduces above 3 GHz in all considered tissues of the heel. Therefore, considering frequencies above 3 GHz for designing an MWI system would not be feasible for bone imaging applications due to the low penetration of EM waves.

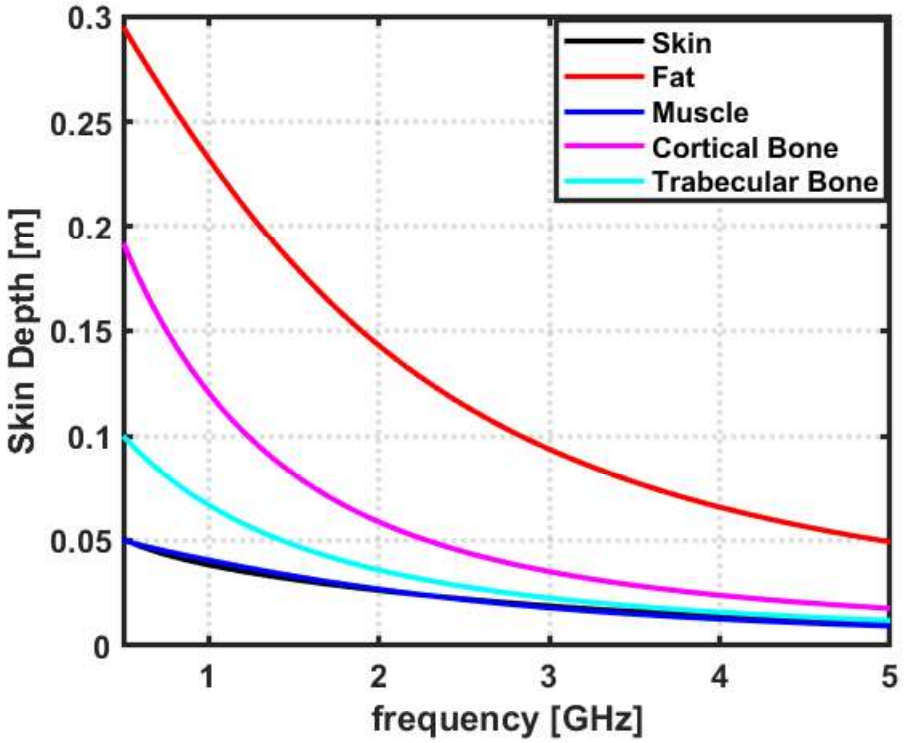

Fig. 7 Skin depth of considered tissues in the human heel. The values are taken from Gabriel *et al*. [14]

2) Cylindrical Layered Model

The waveguide port 1 was excited and the received signal strength at port 2 was analyzed. Both port 1 and port 2 were placed opposite each other, ensuring maximum distance between the ports. Two simulations in CST were performed. The first simulation was performed for a 0.6 – 1.9 GHz frequency band, while, the second simulation was performed for a 2.4 – 3.5 GHz frequency band. The coupling medium used in the simulations has a relative permittivity of 23 and conductivity of 0.005 S/m. Figure 8 shows the comparative analysis of the received signal at port 2 when port 1 was excited. It can be observed from Figure 8, that the received signal at port 2 is significantly high for the frequency band of 0.6 – 1.9 GHz (feasible frequency band) compared to the received signal for the frequency band of 2.4 – 3.5 GHz (inconvenience frequency band). The average percentage difference between the maximum signal for the two cases is found to be 82%, however, the average percentage difference between the minimum signal for the two cases is found to be 88%. As the received signal for the 0.6 – 1.9 GHz frequency band is found to be more compared to the 2.4 – 3.5 GHz frequency band, therefore, our feasibility analysis based on transmission coefficient is validated. Therefore, the upper-frequency range of MWI should be kept below 2 GHz for the maximum received signal.

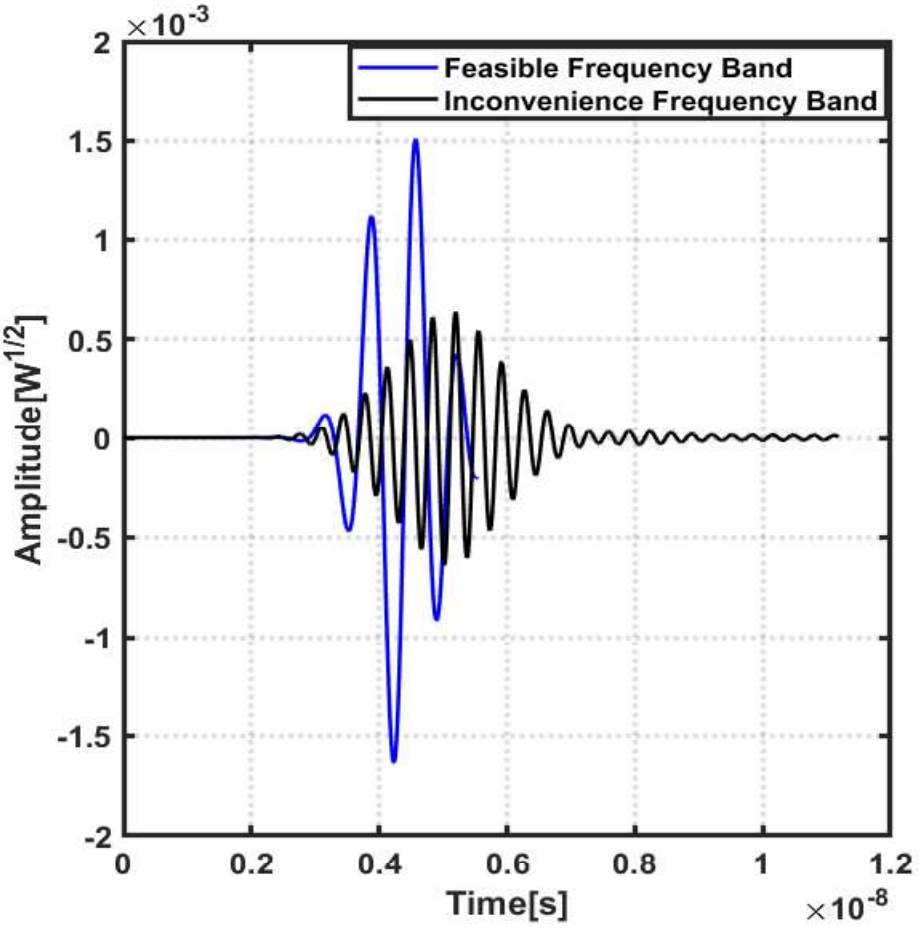

Fig. 8 Port signals for feasible and inconvenience frequency band

An analysis was performed in CST, to analyze the power loss across five-layered medium as a function of frequency. The result of power loss across the five-layered cylindrical model is shown in Figure 9. It can be observed from Figure 9 that the power loss increases in the five-layered cylindrical model as the frequency increases. Thus, for maximum power penetration and minimum power loss for the trabecular bone layer, the operational frequency of the MWI device should be restricted to the lower frequency band.

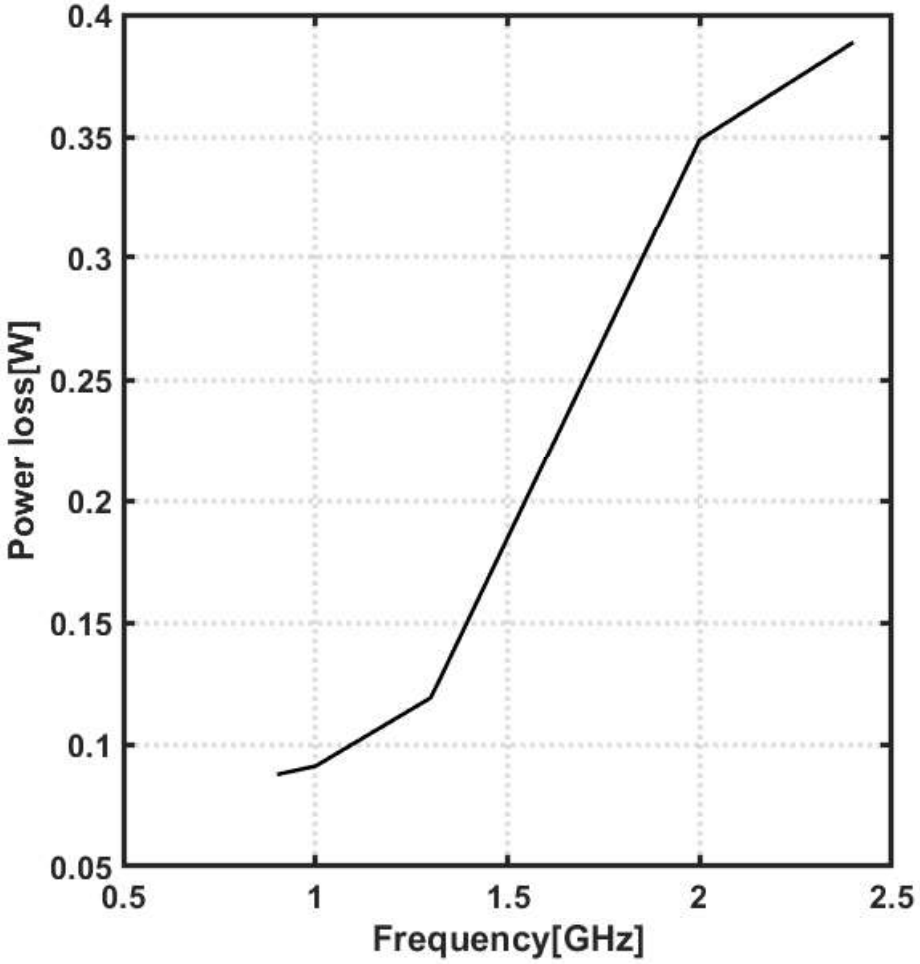

Fig. 9 Power loss in dielectrics for five-layered medium

3) E-field Distribution in Numerical Bone Models

Figure 10(a) shows the z-component of E-field distribution at 1.3 GHz for an osteoporotic numerical bone model. It can be observed from Figure 10(a) that a noticeable amount of E-field penetrates trabecular bone for a five-layered cylindrical model. The penetration of E-field to trabecular bone layer, and hence, the dielectric contrast of the five-layered model suggests enough initial evidence that a dielectric properties map can be generated by applying MWT imaging algorithms on measured EM scattered fields. Moreover, it can also be observed from Figure 10(a) that the skin and muscle layers have higher E-field intensity compared to the trabecular bone layer. This is because these layers have high dielectric properties compared to other layers, therefore, most of the E-field is dissipated in these layers.

Figure 10(b) shows the z-component of E-field distribution at 1.3 GHz for the osteoarthritis numerical bone model. Like the osteoporotic numerical bone model, it can be observed from Figure 10(b) that enough E-field penetrates trabecular bone for the osteoarthritis numerical bone model. Therefore, based on enough E-field penetration both for osteoporotic and osteoarthritis numerical bone models, it can be concluded that the MWT algorithm would be able to classify the numerical bone models based on reconstructed dielectric properties. Similar findings were obtained for the numerical bone model developed by using dielectric properties of trabecular bone acquired from Gabriel *et al*. [15] as shown in Figure 10(c).

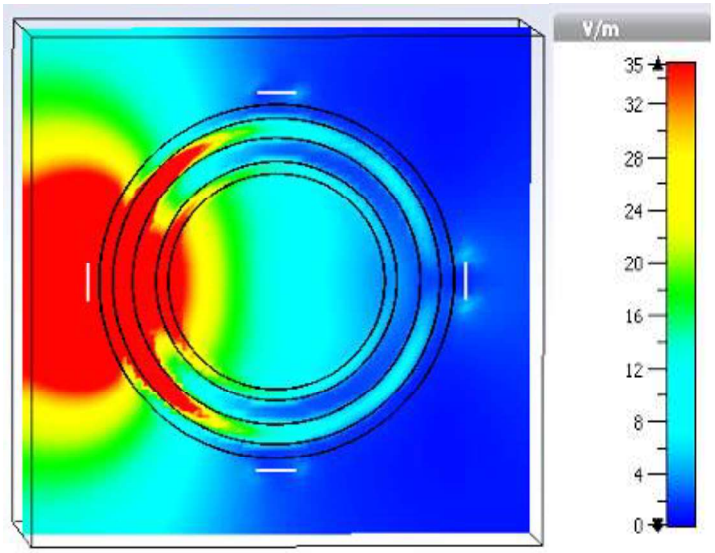
V/m
35
32
28
24
20
16
12
8
4
0

(a)

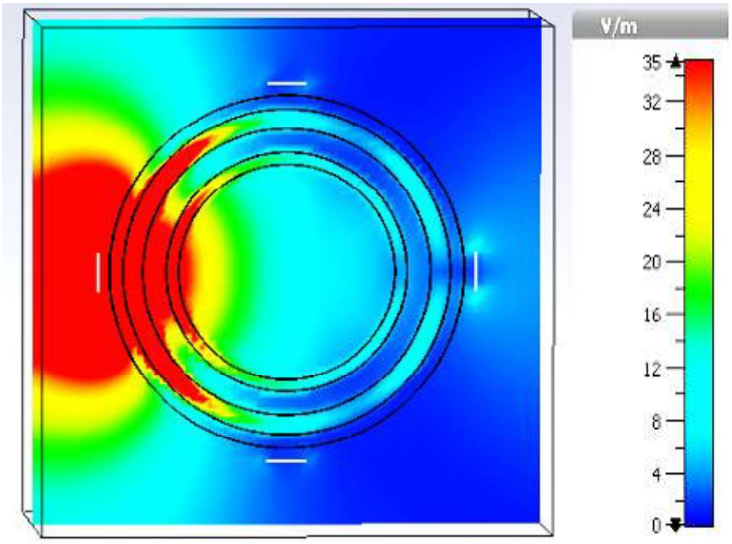
V/m
35
32
28
24
20
16
12
8
4
0

(b)

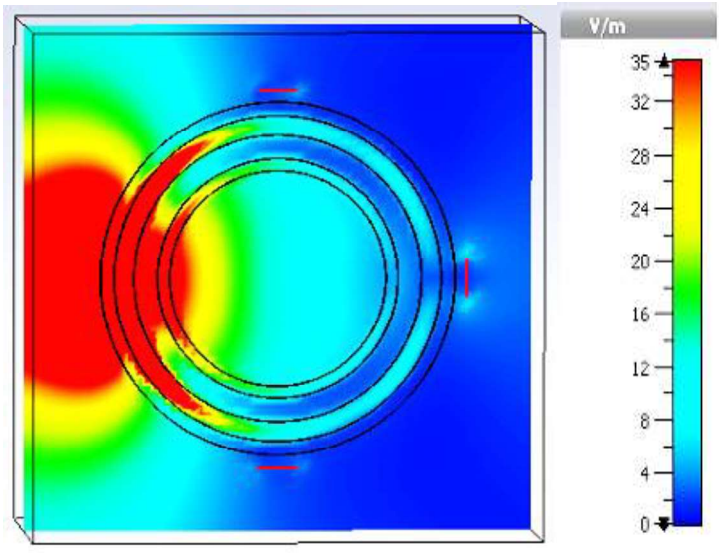
V/m
35
32
28
24
20
16
12
8
4
0

(c)

Fig. 10 Average E-field distribution at 1.3 GHz; **(a)** for Osteoporotic Bone **(b)** for Osteoarthritis Bone **(c)** for Gabriel *et al*. [15]'s Trabecular Bone

4. CONCLUSION

The application of MWI for reconstructing the dielectric properties primarily depends upon the dielectric contrast between tissues of the target anatomical site. Moreover, the spatial resolution of reconstructed images and maximum penetration of EM fields to target tissue primarily depends upon the operational frequency range of the MWI device. This study has made the first attempt towards the investigation of aforementioned constraints before designing of MWI device for monitoring osteoporosis. Firstly, the contrast of dielectric properties of tissues present in the human heel was investigated. Secondly, the TL formalism approach is adopted for finding an optimal selection of frequency band and the corresponding matching medium. Finally, the numerical modelling of the human heel is performed. Based on FDTD simulations performed, the E-field penetration, the received signal strength, and the power loss in the five-layered heel model were analysed. The initial findings from CST simulations on E-field penetration supported the choice of the frequency band by the TL formalism approach. The initial feasibility analysis suggests that the dielectric contrast of the target anatomical site along with the TL formalism approach can be considered as useful tools before designing of MWI system.

These findings support the idea for the development of the MWI device for bone health monitoring. The future work will be based on the development of an MWI prototype for bone imaging. Initially, the MWI system will be tested on bone phantoms. The dielectric properties of bone phantoms will be reconstructed by employing the MWT algorithm. The development of such an MWI device for *in vivo* dielectric properties assessment of bones will help in monitoring the bone quality and hence will provide a low cost, non-invasive, and portable solution for monitoring bone health.

Acknowledgements

The research leading to these results has received funding from the European Research Council under the European Union's Horizon 2020 Programme/ERC Grant Agreement BioElecPro n. 637780 and from the EMERALD project funded from the European Union's Horizon 2020 research and innovation program under the Marie Skłodowska-Curie grant agreement No. 764479. This work is also supported by COST Action MyWAVE CA17115 with an STSM grant entitled "European network for advancing Electromagnetic hyperthermic medical technologies".

Conflict of Interest: The authors declare that they have no conflict of interest.

References

1. Amin B, Elahi MA, Shahzad A et al (2018) Dielectric properties of bones for the monitoring of osteoporosis. Med Biol Eng Comput. https://doi.org/10.1007/s11517-018-1887-z

2. Amin B, Elahi MA, Shahzad A et al (2019) A review of the dielectric properties of the bone for low frequency medical technologies. Biomed Phys Eng Express 5:022001. https://doi.org/10.1088/2057-1976/aaf210

3. Amin B, Kelly D, Shahzad A et al (2020) Microwave calcaneus phantom for bone imaging applications. In: 2020 14th Eur. Conf. Antennas Propag. S 1–5

4. Amin B, Shahzad A, Farina L et al (2019) Investigating human bone microarchitecture and dielectric properties in microwave frequency range. In: 2019 13th Eur. Conf. Antennas Propag. IEEE, S 1–5

5. Amin B, Shahzad A, Farina L et al (2020) Dielectric characterization of diseased human trabecular bones at microwave frequency. In: 2020 Med. Eng. Phys. S 1–8

6. Amin B, Shahzad A, O'halloran M, Elahi MA (2020) Microwave bone imaging: A preliminary investigation on numerical bone phantoms for bone health monitoring. Sensors (Switzerland) 20:1–21. https://doi.org/10.3390/s20216320

7. Bourqui J, Sill JM, Fear EC (2012) A prototype system for measuring microwave frequency reflections from the breast. Int J Biomed Imaging. https://doi.org/10.1155/2012/851234

8. Burge R, Dawson-Hughes B, Solomon DH et al (2007) Incidence and Economic Burden of Osteoporosis-Related Fractures in the United States, 2005-2025. J Bone Miner Res 22:465–475. https://doi.org/10.1359/jbmr.061113

9. Chen H, Zhou X, Fujita H et al (2013) Age-related changes in trabecular and cortical bone microstructure. Int J Endocrinol 2013:213234. https://doi.org/10.1155/2013/213234

10. Cosman F, de Beur SJ, LeBoff MS et al (2014) Clinician's Guide to Prevention and Treatment of Osteoporosis. Osteoporos Int 25:2359–2381. https://doi.org/10.1007/s00198-014-2794-2

11. Cruz AS, Lins HC, Medeiros RVA et al (2018) Artificial intelligence on the identification of risk groups for osteoporosis, a general review. Biomed Eng Online 17:12. https://doi.org/10.1186/s12938-018-0436-1

12. Fajardo JE, Lotto FP, Vericat F et al (2020) Microwave tomography with phaseless data on the calcaneus by means of artificial neural networks. Med Biol Eng Comput 58:433–442

13. Fajardo JE, Vericat F, Irastorza G et al (2019) Sensitivity analysis on imaging the calcaneus using microwaves. Biomed Phys Eng Express. https://doi.org/10.1088/2057-1976/ab3330

14. Gabriel C (2010) Dielectric properties of body tissues in the frequency range 10Hz–100GHz. IFAC (L'Istituto di Fis. Appl. "Nello Carrara") Website

15. Gabriel C, Gabriel S, Corthout E et al (1996) The dielectric properties of biological tissues : III . Parametric models for the dielectric spectrum of tissues The dielectric properties of biological tissues : III . Parametric models for the dielectric spectrum of tissues.

16. Golnabi AH, Meaney PM, Geimer S et al (2011) Microwave tomography for bone imaging. Proc - Int Symp Biomed Imaging 9:956–959. https://doi.org/10.1109/ISBI.2011.5872561

17. Haynes M, Stang J, Moghaddam M (2014) Real-time microwave imaging of differential temperature for thermal therapy monitoring. IEEE Trans Biomed Eng 61:1787–1797. https://doi.org/10.1109/TBME.2014.2307072

18. Irastorza RM, Blangino E, Carlevaro CM, Vericat F (2014) Modeling of the dielectric properties of trabecular bone samples at microwave frequency. Med Biol Eng Comput 52:439–447. https://doi.org/10.1007/s11517-014-1145-y

19. Van Der Linden JC, Weinans H (2007) Effects of microarchitecture on bone strength. Curr Osteoporos Rep 5:56–61. https://doi.org/10.1007/s11914-007-0003-3

20. Lochmüller E-M, Müller R, Kuhn V et al (2003) Can Novel Clinical Densitometric Techniques Replace or Improve DXA in Predicting Bone Strength in Osteoporosis at the Hip and Other Skeletal Sites? J Bone Miner Res 18:906–912. https://doi.org/10.1359/jbmr.2003.18.5.906

21. Makarov SN, Noetscher GM, Arum S et al (2020) Concept of a Radiofrequency Device for Osteopenia / Osteoporosis Screening. :1–15. https://doi.org/10.1038/s41598-020-60173-5

22. Meaney PM, Goodwin D, Golnabi AH et al (2012) Clinical microwave tomographic imaging of the calcaneus: A first-in-human case study of two subjects. IEEE Trans Biomed Eng 59:3304–

3313. https://doi.org/10.1109/TBME.2012.2209202

23. Miller PD, Zapalowski C, Kulak CAM, Bilezikian JP (1999) Bone densitometry: The best way to detect osteoporosis and to monitor therapy. J Clin Endocrinol Metab 84:1867–1871. https://doi.org/10.1210/jc.84.6.1867

24. Njeh CF, Langton CM (1997) The effect of cortical endplates on ultrasound velocity through the calcaneus: an in vitro study. Br J Radiol 70:504–510

25. O'Loughlin D, O'Halloran M, Moloney BM et al (2018) Microwave Breast Imaging: Clinical Advances and Remaining Challenges. IEEE Trans Biomed Eng 65:2580–2590. https://doi.org/10.1109/TBME.2018.2809541

26. Office of the Surgeon General (2004) Bone Health and Osteoporosis - NCBI Bookshelf.

27. Oliveira BL, Halloran MO (2018) Microwave Breast Imaging : Experimental tumour phantoms for the evaluation of new breast cancer diagnosis systems Biomedical Physics & Engineering Related content Microwave Breast Imaging : experimental tumour phantoms for the evaluation of new breast can. https://doi.org/10.1088/2057-1976/aaaaff

28. Oltulu P, Ince B, Kökbudak N et al (2018) Measurement of epidermis, dermis, and total skin thicknesses from six different body regions with a new ethical histometric technique. Turk Plast Rekonstruktif ve Estet Cerrahi Derg 26:56–61. https://doi.org/10.4103/tjps.tjps_2_17

29. Organization WH (2004) WHO SCIENTIFIC GROUP ON THE ASSESSMENT OF OSTEOPOROSIS AT PRIMARY HEALTH Care Level. World Heal Organ May:5–7. https://doi.org/10.1016/S0140-6736(02)08761-5

30. Porter E, Coates M, Popović M (2016) An Early Clinical Study of Time-Domain Microwave Radar for Breast Health Monitoring. IEEE Trans Biomed Eng 63:530–539. https://doi.org/10.1109/TBME.2015.2465867

31. Scapaticci R, Bjelogrlic M, Vasquez JAT et al (2018) Microwave technology for brain imaging and monitoring: physical foundations, potential and limitations. In: Emerg. Electromagn. Technol. Brain Dis. Diagnostics, Monit. Ther. Springer, S 7–35

32. Scapaticci R, Di Donato L, Catapano I, Crocco L (2012) A feasibility study on microwave imaging for brain stroke monitoring. Prog Electromagn Res 40:305–324

33. Shahzad A, O'Halloran M, Jones E, Glavin M (2016) A multistage selective weighting method for improved microwave breast tomography. Comput Med Imaging Graph 54:6–15. https://doi.org/10.1016/j.compmedimag.2016.08.007

34. Slaney M, Kak AC, Larsen LE (1984) Limitations of Imaging with First-Order Diffraction Tomography. IEEE Trans Microw Theory Tech 32:860–874. https://doi.org/10.1109/TMTT.1984.1132783

35. Topoliński T, Mazurkiewicz A, Jung S et al (2012) Microarchitecture parameters describe bone structure and its strength better than BMD. Sci World J. https://doi.org/10.1100/2012/502781

36. Vogel JM, Wasnich RD, Ross PD (1988) The clinical relevance of calcaneus bone mineral measurements: a review. Bone Miner 5:35–58. https://doi.org/10.1016/0169-6009(88)90005-0

Author biography